Correlated insulating states in carbon nanotubes controlled by magnetic field

Assaf Voliovich,[1] Mark S. Rudner [●],[2,3] Yuval Oreg,[1] and Erez Berg[1]

[1]*Department of Condensed Matter Physics, Weizmann Institute of Science, Rehovot 76100, Israel*
[2]*Department of Physics, University of Washington, Seattle, Washington 98195-1560, USA*
[3]*Niels Bohr Institute, University of Copenhagen, 2100 Copenhagen, Denmark*

We investigate competing insulating phases in nearly metallic zigzag carbon nanotubes, under conditions where an applied magnetic flux approximately closes the single-particle gap in one valley. Recent experiments have shown that an energy gap persists throughout magnetic field sweeps where the single-particle picture predicts that the gap should close and reopen. Using a bosonic low-energy effective theory to describe the interplay between electron-electron interactions, spin-orbit coupling, and magnetic field, we obtain a phase diagram consisting of several competing insulating phases that can form in the vicinity of the single-particle gap closing point. We characterize these phases in terms of spin-resolved charge polarization densities, each of which can independently take one of two possible values consistent with the mirror symmetry of the system, or can take an intermediate value through a spontaneous mirror symmetry breaking transition. In the mirror symmetry breaking phase, adiabatic changes of the orbital magnetic flux drive charge and spin currents along the nanotube. We discuss the relevance of these results to recent and future experiments.

I. INTRODUCTION

Carbon nanotubes (CNTs) offer a versatile platform for studying the exotic quantum many-body physics of one-dimensional (1D) electronic systems. A variety of intriguing phenomena have been observed, including Wigner crystal formation [1] and possible Luttinger liquid behavior [2], strong [3], and spatially resolved [4] electron-phonon coupling [5,6], and highly efficient multiple carrier generation through photoexcitation cascade [7]. Despite the extremely weak spin-orbit coupling (SOC) in graphene, the parent material for CNTs, remarkably strong SOC has been observed [8,9] and exploited for spin qubit operation [10–12] while also providing means for efficient spin relaxation [13–16] and nanomechanical coupling [17].

At the single-particle level, the electronic structure of a CNT is determined by its diameter, d, and chirality, i.e., the orientation of the honeycomb lattice of carbon atoms relative to the nanotube axis [18]. Here we focus on nominally metallic zigzag CNTs, as illustrated in Fig. 1(a). In such CNTs, the combination of quantization of the circumferential wave vector k_c and curvature-induced strain yield low-energy one-dimensional subbands with small gaps that decay systematically with CNT diameter as $\sim 1/d^2$ (see Fig. 1(b) and Refs. [19,20]). By applying a magnetic flux, Φ, through the nanotube, these 1D subbands can be shifted relative to the Dirac points of the underlying two-dimensional graphene dispersion, in principle allowing the gap to be closed in one valley at a critical value of the applied flux, Φ_c [Figs. 1(b) and 1(c)].

Intriguingly, experiments on ultraclean, suspended small-gap CNTs have shown that while the gap can be tuned by applied flux, the minimal gap achieved during continuous sweeps (where the gap first shrinks and then grows again) generically retains a significant nonzero value (of order a few tens of meV) [21]. This failure of the single-particle picture to account for the observed behavior suggests that electron-electron interactions (which are essentially unscreened at charge neutrality in suspended devices) may dramatically transform the nature of the ground state in this regime. Theoretical studies have predicted various interaction-driven insulating states in carbon nanotubes [22–27].

In this work, we investigate the effects of electron-electron interactions on the ground states of nominally metallic carbon nanotubes. We find that the system obtains one of several competing insulating ground states, controlled by the interplay between spin-orbit coupling, magnetic field, and interactions. To characterize these states we introduce the "spin-resolved charge polarization densities," P_σ. Here, $\sigma = \uparrow, \downarrow$ indicates the spin direction relative to the quantization axis along the nanotube, which we denote by $\hat{x}$. The spin-resolved polarization densities are illustrated schematically in Fig. 1(d). In preserving the mirror symmetry of the zigzag nanotube [reflection across a mirror plane M_x that bisects the longitudinal bonds shown in red in Fig. 1(a)], each polarization component can obtain one of two possible values, 0 or 1/2. In the absence of interactions, these two cases correspond to Wannier centers for spin-up and spin-down electrons positioned on the longitudinal (red) or "diagonal" (blue) bonds of the CNT shown in Fig. 1(a). We further show that under certain conditions, states which spontaneously break the mirror symmetry may be favored, where $P_{\uparrow,\downarrow}$ are neither 0 nor 1/2. To the best of our knowledge, this is the first prediction and discussion of a possible mirror symmetry breaking phase promoted by the
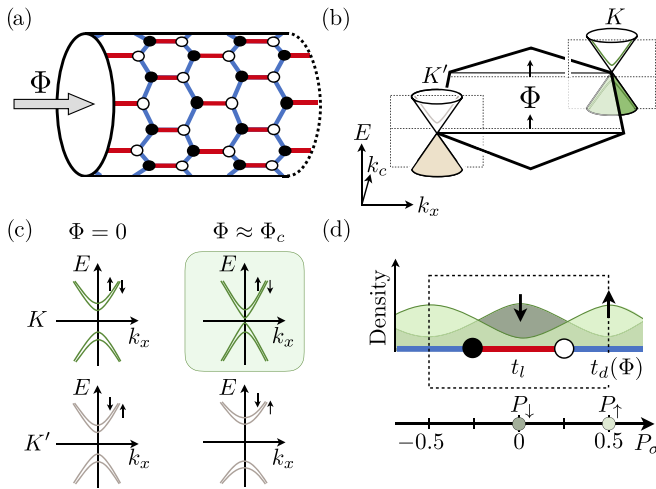
FIG. 1. Competing insulating phases of a nearly metallic zigzag carbon nanotube (CNT). (a) Geometry of the CNT. A magnetic flux Φ threaded through the CNT tunes the one-dimensional electronic subband dispersion [(b) and (c)]. Filled (empty) circles indicate A (B) sites. (b) Two-dimensional graphene Brillouin zone and low-energy dispersion, with the lowest one-dimensional sub-band sections of the CNT indicated. While geometric quantization of the circumferential wave number k_c would suggest that the CNT should be metallic, curvature of the CNT offsets the subbands from the Dirac points (dashed lines), leading to a small single-particle gap that can be controlled by the flux, Φ. (c) Lowest subband dispersion relations in valleys K and K', at zero flux ($\Phi = 0$) and near the critical flux ($\Phi \approx \Phi_c$). Our analysis focuses on the effective one-dimensional system comprised of the low-energy modes for $\Phi \approx \Phi_c$, highlighted by the green box. (Here we assume that the zero flux gap due to curvature/strain is larger than the SOC strength.) (d) Distinct insulating phases are characterized by the spin-resolved charge polarization densities, $P_\uparrow$ and $P_\downarrow$, shown here with a relative offset of one half unit cell as in the phase realized at large spin-orbit coupling, λ, see Fig. 2(a).

interplay of Coulomb interactions and spin-orbit coupling in CNTs.

II. PHYSICAL PICTURE

Before beginning our detailed analysis, we give a simple physical picture that helps to motivate our results. As discussed, for example, in the supplementary material of Ref. [28] and illustrated in Figs. 1(a) and 1(d), the single-particle electronic states in one valley of a zigzag CNT, for each spin species, can be described via a mapping to the Su-Schrieffer-Heeger (SSH) model of polyacetylene [29]. In Fig. 1(a), we identify two types of bonds: "longitudinal bonds" that run parallel to the nanotube axis (shown in red color) and "diagonal bonds" which have components oriented around its circumference (shown in blue color). The low-energy electronic states in the K and K' valleys are described by large values of the circumferential wave-vector component k_c [Fig. 1(b)].

Fixing k_c to the value corresponding to K or K' yields an effective 1D tight binding model [Fig. 1(d)] with alternating hopping amplitudes t_ℓ and t_d arising from the longitudinal and diagonal bonds, respectively. For a flat sheet of graphene and

in the absence of a magnetic field, the hopping amplitudes are identical along all bonds. For the CNT, the combination of phases arising from circumferential motion ($k_c \neq 0$), curvature-induced strain, magnetic flux, and spin-orbit coupling affects the interference between amplitudes for hopping along the two diagonal bonds entering each site; in particular, this allows the *magnitude* of the hopping amplitude $t_d(\Phi)$ in the effective 1D model to be tuned by the flux Φ.

Using the flux tunability of $t_d(\Phi)$, various regimes of effective dimerization can be explored. For a noninteracting system, these correspond to cases where the Wannier centers for electrons in the low-energy spin-up and spin-down bands can independently be centered either on the longitudinal or the diagonal bonds. In a many-body setting at charge neutrality, these situations correspond to insulating phases with charge polarization densities P_σ for spin-up ($\sigma = \uparrow$) and spin-down ($\sigma = \downarrow$) electrons taking values 0 or 1/2 (in units of the electron charge, e), see Fig. 1(d). With interactions there is an additional possibility of spontaneous mirror symmetry breaking, where at least one of the P_σ's takes a value different from 0 and 1/2. Moreover, interactions can shift phase boundaries and renormalize energy gaps, the spin-orbit coupling, and the orbital moments in each valley. Below we treat the interacting problem in detail and map out the resulting phase diagram of the system (see Fig. 2).

III. MODEL

To analyze the low-energy behavior of the system, we use a one-dimensional continuum model. The model describes the (spinful) electrons in the lowest energy sub-band of a single valley, in which the single-particle gap is nearly closed by an applied magnetic flux [shaded panel in Fig. 1(c)]. Within this model the Hamiltonian takes the form (with $\hbar = 1$ throughout, unless otherwise noted):

$$\mathcal{H} = \int dx \Bigg[-v \sum_{\sigma,r} r \psi_{r\sigma}^\dagger i \partial_x \psi_{r\sigma} - \sum_{\sigma,r} (h\sigma + \mu) \rho_{r\sigma}$$
$$+ \sum_\sigma \frac{2v}{d} (\lambda\sigma - f)(i\psi_{R\sigma}^\dagger \psi_{L\sigma} + \text{H.c.}) \Bigg] + \mathcal{H}_{\text{int}}, \quad (1)$$

where v is the Fermi velocity, d is the nanotube's diameter, $\psi_{r\sigma}^\dagger$ ($\psi_{r\sigma}$) is the creation (annihilation) operator of a left ($r = L$) or right ($r = R$) moving electron with spin $\sigma = \uparrow, \downarrow$ at position x, $\rho_{r\sigma} = \psi_{r\sigma}^\dagger \psi_{r\sigma}$, and $\mathcal{H}_{\text{int}}$ describes the electron-electron interaction, to be defined below. (When it is not used as a subscript, we assign $\sigma = +1$ for spin up and $\sigma = -1$ for spin down; similarly, we let $r = +$ for right movers and $r = -$ for left movers, and $\bar{r} = -r$.) The coefficient $\frac{2v}{d}(\lambda\sigma - f)$ is the spin-dependent mass arising due to a combination of spin-orbit coupling, λ, and the normalized orbital flux, $f = \frac{\Phi - \Phi_c}{2\pi\hbar/e}$. The Zeeman energy due to the application of the axial field is denoted by h, and μ is the chemical potential.

The CNT is invariant under a mirror reflection M_x with respect to a plane perpendicular to the nanotube axis that passes through the middle of the longitudinal bonds (red color in Fig. 1). To see how this symmetry is manifested in our description, it is helpful to recall that, microscopically, the right- and left-mover single-particle states have a pseudospin

structure described by particular sets of amplitudes on the A and B sublattices of carbon atoms. Specifically, due to the zigzag CNT's geometry and for our choice of basis, these amplitudes correspond to the eigenstates of the second (i.e., y) Pauli matrix in the sublattice space; consequently, electronic states supported on the A and B sublattices are created by the operators $\psi_{A\sigma}^\dagger = \frac{1}{\sqrt{2}}(\psi_{R\sigma}^\dagger + \psi_{L\sigma}^\dagger)$, $\psi_{B\sigma}^\dagger = -\frac{1}{i\sqrt{2}}(\psi_{R\sigma}^\dagger - \psi_{L\sigma}^\dagger)$, respectively. Noting that the A and B sublattices are interchanged by the mirror operation M_x, $\psi_A^\dagger \leftrightarrow \psi_B^\dagger$, the relations above determine that this symmetry acts as $\psi_{R\sigma} \to i\psi_{L\sigma}$, $\psi_{L\sigma} \to -i\psi_{R\sigma}$. It is straightforward to check that all terms in Eq. (1) are invariant under this symmetry.

We describe the electron-electron Coulomb interaction, which we assume to be screened by a nearby metallic gate,[1] via

$$\mathcal{H}_{\text{int}} = \frac{1}{2}\sum_{\alpha\beta}\int dx \int dx' U_{\alpha\beta}(x-x') :\rho_\alpha(x)\rho_\beta(x'): , \quad (2)$$

where $\alpha, \beta = \{A, B\}$ are sublattice indices, $\rho_\alpha(x) = \sum_\sigma \psi_{\alpha,\sigma}^\dagger \psi_{\alpha,\sigma}$, and $:O:$ denotes normal ordering of the operator O relative to the (noninteracting) Fermi sea. Here $U_{AA}(x-x') = U_{BB}(x-x')$ describes the interaction between two electrons on the same sublattice, whereas $U_{AB}(x-x') = U_{BA}(x-x')$ is the interaction between electrons on different sublattices.

To treat the interacting system, we bosonize the Hamiltonian in Eq. (1) following the standard procedure [30]. We first introduce canonical bosonic fields θ_σ, ϕ_σ, satisfying the commutation relations $[\phi_\sigma(x), \theta_{\sigma'}(x')] = i\pi\delta_{\sigma\sigma'}\Theta(x'-x) + i\pi(1-\delta_{\sigma\sigma'})$. The electronic field operator is written as $\psi_{r\sigma} = \frac{1}{\sqrt{2\pi d}}e^{i(\theta_\sigma + r\phi_\sigma)}$, and the density of the electrons with spin σ is given by

$$\rho_\sigma = \frac{1}{\pi}\partial_x\phi_\sigma. \quad (3)$$

We decompose the Hamiltonian into four contributions:

$$H = H_0 + H_Z + H_{\lambda,f} + H_{\text{BS}}, \quad (4)$$

where H_0 captures the electronic kinetic energy (neglecting spin-orbit coupling and orbital coupling to the applied magnetic flux) as well as the forward scattering part of the electron-electron interaction, H_Z describes the Zeeman coupling and chemical potential, $H_{\lambda,f}$ captures the spin-orbit and orbital magnetic couplings, and H_{BS} captures the backscattering part of the electron-electron interaction.

For analyzing the bosonized Hamiltonian, it is convenient to introduce spin (s) and charge (c) fields: $\phi_j = \frac{1}{\sqrt{2}}(\phi_\uparrow + \eta_j\phi_\downarrow)$ and $\theta_j = \frac{1}{\sqrt{2}}(\theta_\uparrow + \eta_j\theta_\downarrow)$, where $j = c, s$ and $\eta_c = +1$, $\eta_s = -1$. In terms of these new fields, we have [30]

$$H_0 = \sum_{j=c,s}\frac{v_j}{2\pi}\int dx\left[K_j(\partial_x\theta_j)^2 + \frac{1}{K_j}(\partial_x\phi_j)^2\right], \quad (5)$$

with $v_j = v(1 + \frac{U_+(1+\eta_j)/2 + U_-\eta_j}{\pi v})^{1/2}$ and $K_j = v/v_j$, where $U_\pm = \frac{1}{2}\int dx(U_{AA} \pm U_{AB})$. The interaction U_+ corresponds to forward-scattering processes and is typically larger than U_- by a factor of the order of d/a, where a is the lattice spacing [31]. The Zeeman and chemical potential terms are given by

$$H_Z = -\int dx\left(\mu\frac{\sqrt{2}}{\pi}\partial_x\phi_c + h\frac{\sqrt{2}}{\pi}\partial_x\phi_s\right), \quad (6)$$

while the mass terms due to spin-orbit coupling and the magnetic flux are written as

$$H_{\lambda,f} = -\frac{2v}{\pi d^2}\int dx[\lambda\sin(\sqrt{2}\phi_s)\sin(\sqrt{2}\phi_c) + f\cos(\sqrt{2}\phi_s)\cos(\sqrt{2}\phi_c)]. \quad (7)$$

Finally, the backscattering interaction terms are given by

$$H_{\text{BS}} = \frac{v}{\pi d^2}\int dx[g_s\cos(2\sqrt{2}\phi_s) - g_c\cos(2\sqrt{2}\phi_c)], \quad (8)$$

where $g_s = g_c = \frac{U_-}{2\pi v} > 0$. In the following, we study the insulating ground states realized in this model as λ, f, h, and μ are tuned.

IV. POLARIZATION

The insulating states of the nanotube are most conveniently characterized by the values of the electric polarizations [32–36] of spin up and spin down electrons. A boundary between two states with different polarizations hosts a fractional charge and/or fractional spin, equal to the difference of the polarization densities in the two states.

Our goal in this section is to relate the spin-resolved polarization densities $\{P_\sigma\}$ of an insulating state to its bosonized description, in which the fields ϕ_σ are pinned to certain values. Heuristically, a relation between P_σ and $\langle\phi_\sigma\rangle$ can be derived by noting that, in the bosonized description, the charge densities are given by Eq. (3). Therefore the total charge of spin σ at the boundary between two insulating phases where ϕ_σ is pinned to $\phi_{1,\sigma}$ and $\phi_{2,\sigma}$ is given by $\langle\int dx\rho_\sigma(x)\rangle = \frac{1}{\pi}\langle\phi_{2,\sigma} - \phi_{1,\sigma}\rangle$, where the integral is performed over a region that includes the boundary. On the other hand, since by definition $\partial_x P_\sigma = \langle\rho_\sigma\rangle$, we infer that $P_\sigma = \frac{1}{\pi}\langle\phi_\sigma\rangle + P_0$, where P_0 is a constant. Notice that, since $\langle\phi_\sigma\rangle$ in an insulator is defined modulo π, P_σ is defined up to an integer [32]. Within our conventions, under mirror reflection M_x, $\phi_\sigma \to -\phi_\sigma$. It is therefore natural to choose $P_0 = 0$, such that under M_x, $P_\sigma \to -P_\sigma$. With this choice, we express P_σ in terms of the charge and spin fields as

$$P_\uparrow = \frac{1}{\pi\sqrt{2}}(\phi_c + \phi_s),$$

$$P_\downarrow = \frac{1}{\pi\sqrt{2}}(\phi_c - \phi_s). \quad (9)$$

There are two distinct values for P_σ that are invariant under M_x: $P_\sigma = 0$ and $1/2$ (mod 1). As noted in Ref. [28], this implies that there are four different band insulating phases that respect the mirror symmetry. These phases can be accessed by tuning the axial magnetic field and (in principle) the spin-orbit coupling. In the presence of interactions, phases that break the
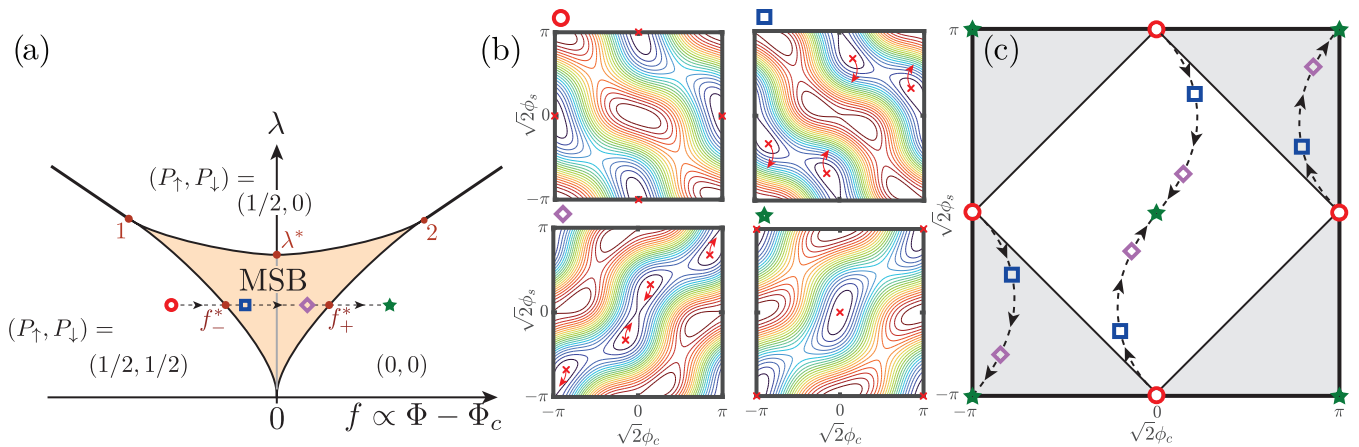
---

[1]While our analysis does not depend on the detailed functional forms of the interaction potentials $U_{AA}(x-x')$ and $U_{AB}(x-x')$, screening is important to ensure that the interaction parameter U_+ defined below Eq. (5) is finite.

FIG. 2. Correlated insulating phases of a zigzag carbon nanotube, described the Hamiltonian in Eqs. (4) to (8). (a) Phase diagram as a function of orbital magnetic flux $f \propto \Phi - \Phi_c$ and spin-orbit coupling, λ, at zero Zeeman field and chemical potential, $h = \mu = 0$. Gapped phases that respect the mirror symmetry of the CNT are labeled by corresponding values of the spin-resolved polarization densities, $P_\uparrow = \frac{1}{\pi\sqrt{2}}(\phi_c + \phi_s)$ and $P_\downarrow = \frac{1}{\pi\sqrt{2}}(\phi_c - \phi_s)$. Due to electron-electron interactions, a mirror symmetry breaking (MSB) phase appears over a finite range of flux and spin-orbit coupling. The polarization densities take nonuniversal values within the MSB phase. Adiabatically changing the flux along the dashed line within this phase drives spin and charge currents through the CNT, realizing a magnetoelectric effect. (b) Four representative snapshots of the potential landscape for the spin and charge fields, ϕ_s and ϕ_c, resulting from spin-orbit coupling and the orbital magnetic flux, $H_{\lambda,f}$ in Eq. (7), and backscattering interactions, H_{BS} in Eq. (8). Blue (red) colors represented lower (higher) potential. The parameters used in the plots are: $g_c = g_s = \lambda/3$ and $f = -2\lambda, -1.17\lambda, 1.17\lambda, 2\lambda$ for the points denoted by the red circle, blue square, purple diamond, and green star, respectively. The corresponding points in the phase diagram in panel (a) are marked by the colored symbols. Locations of the potential minima are marked by red crosses; points separated by (π, π) represent equivalent physical states. Red arrows indicate the direction of motion of the potential minima as the flux f is scanned across the dashed line through the MSB phase, revealing how charge and spin are driven through the CNT as f is varied adiabatically. (c) Motion of the minima along the dashed line in (a). Points in the white region correspond to physically distinct states. Notice that the minimum corresponding to the red circles remains at $(0, \pi)$ throughout the phase characterized by $(P_\uparrow, P_\downarrow) = (1/2, 1/2)$, and similarly for the minimum corresponding to the green star.

mirror symmetry spontaneously are also possible. Below, we study the phase diagram of the system with interactions, using the polarization densities $\{P_\sigma\}$ to label the distinct phases.

V. PHASE DIAGRAM

As a first step, we focus on the phase diagram as a function of the two mass terms, f and λ, at charge neutrality, $\mu = 0$, and in the absence of a Zeeman field, $h = 0$ (the effect of the Zeeman coupling h will be considered below). At the point $\lambda = f = 0$, the coupling between the spin and charge fields in Eq. (7) vanishes, and the spin and charge sectors decouple from each other. In the charge sector, the Hamiltonian is of the standard sine-Gordon form. The term proportional to g_c in Eq. (8) is relevant for repulsive interactions ($K_c < 1$). This term pins $2\sqrt{2}\phi_c$ to zero (mod 2π) and opens a charge gap, $\Delta_c \sim \frac{v}{d} g_c^{\frac{1}{2-2K_c}}$. We consider the case where ϕ_c is pinned to zero here; it is straightforward to check that other choices (e.g., $2\sqrt{2}\phi_c = 2\pi$) lead to identical physical predictions, and in fact correspond to the *same* ground state. However, with $\lambda = 0$ the system is SU(2) symmetric (recall that for now, we are considering $h = 0$); in this case g_s is marginally irrelevant [30] and the fixed point is given by $g_s = 0$, $K_s = 1$. Therefore the spin sector is gapless at the point $\mu = h = \lambda = f = 0$.

A. Phases along the flux axis: $f \neq 0, \lambda = 0$

We now consider the effect of the mass terms λ and f, keeping for simplicity $h = 0$. Turning on $f \neq 0$ opens a gap

in the spectrum, whose scaling with f depends on the interaction strength [37]. We may use the fact that ϕ_c is pinned to zero to replace $\cos(\sqrt{2}\phi_c)$ in Eq. (7) by its expectation value (reduced from 1 due to the fluctuations of ϕ_c). The remaining $\cos(\sqrt{2}\phi_s)$ is relevant, and gives rise to a spin gap $\Delta_f \sim \frac{v}{d}|f|^{2/3}$,[2] up to logarithmic corrections (due to the presence of the marginally irrelevant g_s term). The value obtained by ϕ_s depends on the sign of f: to minimize the energy, $\sqrt{2}\phi_s = 0$ (mod 2π) for $f > 0$ and $\sqrt{2}\phi_s = \pi$ (mod 2π) for $f < 0$.

Using the relations between ϕ_c, ϕ_s, and P_σ in Eq. (9), we find that the phase obtained for $\lambda = 0$, $f \neq 0$ is described by $P_\uparrow = P_\downarrow = 0$ for $f > 0$, or $P_\uparrow = P_\downarrow = 1/2$ (mod 1) for $f < 0$. This behavior is as expected based on the analogy to the SSH model described in Sec. II and in Ref. [28], in which the Wannier centers of spin-up and spin-down electrons would both be located either on the horizontal or the diagonal bonds of the zigzag CNT [see Fig. 1(a)].

B. Phases along the axis $f = 0, \lambda \neq 0$

We now investigate the effect of spin-orbit coupling, focusing on the axis $f = 0, \lambda \neq 0$. First consider the limit of very strong spin-orbit coupling, $|\lambda| \gg g_{c,s}$ (i.e., where the backscattering interactions H_{BS} can be neglected). For $\lambda > 0$,

---

[2]Unlike Ref. [37], here we are assuming that the charge mode is gapped due to the g_c (backscattering) term, resulting in a different scaling of the gap with f.

ϕ_c and ϕ_s become pinned to values such that $\sin(\sqrt{2}\phi_c) = \sin(\sqrt{2}\phi_s) = \pm 1$, i.e., $\sqrt{2}\phi_c = \sqrt{2}\phi_s = \pi/2$ (mod 2π) or $\sqrt{2}\phi_c = \sqrt{2}\phi_s = 3\pi/2$ (mod 2π). These values correspond to spin-resolved polarization densities $P_\uparrow = 1/2$, $P_\downarrow = 0$ (mod 1), as shown in Fig. 1(d); in the SSH analogy, spin-orbit coupling produces opposite dimerization patterns for spin-up and spin-down electrons [28]. For $\lambda < 0$, $P_\uparrow$ and $P_\downarrow$ are reversed.

Now consider the opposite limit, where a very weak spin-orbit coupling is introduced on top of the gapless state at $\mu = h = \lambda = f = 0$. Since ϕ_c is pinned to zero by $H_{\rm BS}$ as described above, the $\lambda \sin(\sqrt{2}\phi_s)\sin(\sqrt{2}\phi_c)$ term in $H_{\lambda,f}$ may appear to be unimportant. However, to second order in λ, after integrating out the fluctuations of the massive ϕ_c field, we obtain a correction to g_s of the form $\delta g_s \sim |A|\lambda^2$, where $A \sim K_c \ln(g_c K_c)$. This correction breaks the SU(2) symmetry in the spin sector, and makes g_s marginally relevant.[3] As a result, a gap $\Delta_\lambda \sim \frac{v}{d}\exp(-1/\sqrt{2g_s\delta g_s})$ opens in the spin sector, and $2\sqrt{2}\phi_s$ is pinned to a value $(2m+1)\pi$, where m is an integer.

In order to interpret the gapped phase that arises for $f = 0$, $0 < |\lambda| \ll g_{c,s}$, we examine the sublattice magnetization operator: $\mathcal{O}_s = \sum_\sigma \sigma(\psi_{A\sigma}^\dagger \psi_{A\sigma} - \psi_{B\sigma}^\dagger \psi_{B\sigma}) \sim -\frac{4}{d}\sin(\sqrt{2}\phi_s)\cos(\sqrt{2}\phi_c)$. This operator is odd under mirror symmetry. In the $f = 0$, $0 < |\lambda| \ll 1$ phase, $\langle \mathcal{O}_s \rangle \neq 0$, and mirror symmetry is spontaneously broken. Notice that depending on whether m is an even or an odd integer, the sign of $\langle \mathcal{O}_s \rangle$ is either negative or positive, respectively. These two possibilities reflect the two expected degenerate ground states that arise from spontaneously breaking the mirror symmetry.

To analyze how the large and small $|\lambda|$ limits are connected, notice that both the backscattering interaction term and the spin-orbit term are minimized for $\sqrt{2}\phi_s = \pi/2$ (mod π), just as in the strong spin-orbit phase described above. Thus ϕ_s may remain constant throughout the parameter regime between the small and large $|\lambda|$ limits. However, when the spin-orbit interaction is the dominant energy scale, $\sqrt{2}\phi_c$ becomes pinned to $\pm\pi/2$ (depending on whether the integer m defined above is even or odd), rather than to 0 as in the small spin-orbit limit. Therefore, due to the competition between the g_c term in $H_{\rm BS}$ and the λ term in $H_{\lambda,f}$, we expect $\sqrt{2}\phi_c$ to continuously change from 0 to $\pm\pi/2$ as $|\lambda|$ is increased from 0. Correspondingly, the polarization densities evolve continuously from $P_\uparrow = \pm 1/4$, $P_\downarrow = \mp 1/4$ to $P_\uparrow = 1/2$, $P_\downarrow = 0$ as we move up along the λ axis. In accordance with the comments about sublattice magnetization above, the polarization density values $P_\uparrow = \pm 1/4$, $P_\downarrow = \mp 1/4$ are indicative of a state where spin-up and spin-down electrons each exhibit unequal populations on the atomic A and B sublattices of the CNT. We denote the critical value of λ at which $\sqrt{2}\phi_c$ reaches zero as λ^* [see Fig. 2(a)]; for $\lambda > \lambda^*$, the mirror symmetry is restored.

C. Phase structure for $f \neq 0, \lambda \neq 0$

Next, we discuss the phase diagram with nonzero f and λ, keeping $h = \mu = 0$. As discussed above, along the axis $f = 0$, $\lambda > 0$ there is a gapped phase that spontaneously breaks the mirror symmetry of the system. We consider a cut through the phase diagram, varying f at a fixed nonzero value of $\lambda < \lambda^*$ [dashed line in Fig. 2(a)]. In Fig. 2(b), we show the potential given by $H_{\lambda,f} + H_{\rm BS}$ [Eqs. (7) and (8)] as a function of $\sqrt{2}\phi_c$ and $\sqrt{2}\phi_s$ at four representative points along the dashed line. The red crosses in the figure indicate the minima of the potential. Notice that points separated by $(\pm\pi, \pm\pi)$ have the same values of $P_\uparrow$ and $P_\downarrow$ (mod integer), and hence describe the same physical state.

At the point in the phase diagram [Fig. 2(a)] marked by a red circle, the corresponding potential in Fig. 2(b) has a minimum at $(\pi, 0)$, corresponding to a polarization $(P_\uparrow, P_\downarrow) = (1/2, 1/2)$. Beyond $f = f_-^*$, this minimum splits into two minima, as shown for the point indicated by the blue square in Fig. 2(a). These minima move away from each other and towards $(\phi_c, \phi_s) = (0, 0)$ as f increases [see arrows indicating the direction of motion for the potential minima, and the potential corresponding to the point marked by purple diamond in Fig. 2(b)], until they merge at $(\phi_c, \phi_s) = (0, 0)$ when $f = f_+^*$. Beyond this point, the minimum is at the origin, corresponding to a polarization $(P_\uparrow, P_\downarrow) = (0, 0)$ (see potential at the point marked by the green star). Figure 2(c) shows the motion of the potential minima along the dashed line in Fig. 2(a).

Within the mirror symmetry breaking (MSB) phase [filled region in Fig. 2(a)], both ϕ_c and ϕ_s change continuously as f is varied, corresponding to changes in the polarization densities $P_{\uparrow,\downarrow}$. Therefore an adiabatic change in the axial field within this phase causes spin and charge currents to flow along the nanotube. As f changes from f_-^* to f_+^*, $\sqrt{2}\phi_s$ changes by $\pm\pi$. This change of ϕ_s corresponds to one net electron spin being pumped across the system. The direction of the pumping depends on which of the two degenerate grounds states the system is in. Additionally, ϕ_c also changes as f varies from f_-^* to f_+^* [see potentials corresponding to the blue square and purple diamond, displayed in Figs. 2(b) and 2(c)]. These changes of ϕ_c imply that the charge polarization density changes as the magnetic field is varied, realizing a magneto-electric effect. Unlike ϕ_s, the change of ϕ_c is nonmonotonic, with no net charge being pumped as f changes from f_-^* to f_+^*. The maximum change in the charge polarization is obtained at an intermediate value of the flux within the MSB phase. Its magnitude is nonuniversal, depending on microscopic parameters such as λ, g_c, and the Luttinger parameter K_c.

For a sufficiently large λ, the MSB phase disappears for all values of f. Instead, there is a direct transition from the $(P_\uparrow, P_\downarrow) = (1/2, 1/2)$ phase to the $(1/2, 0)$ phase, and another transition from the $(1/2, 0)$ phase to the $(0, 0)$ phase, as in the noninteracting case [28]. Across these transitions, the charge polarization density changes discontinuously by $1/2$. Along the transition lines [the thick black lines emanating from the points 1 and 2 in Fig. 2(a)] the interaction terms in Eq. (8) are irrelevant. At points 1 and 2, the interaction terms are marginal. Between these points, each transition line splits in two, and the MSB phase is formed. The boundaries of the

---

[3] In addition to the renormalization of g_s, integrating out the fluctuations of ϕ_c also renormalizes K_s upward. This increase of the spin stiffness together with the increase of g_s helps pin the value of ϕ_s.

MSB phase (except the points 1, 2, and the origin) are likely to be of the 1+1 dimensional Ising universality class, since along these lines the $\mathbb{Z}_2$ mirror symmetry is broken.

D. Effect of the Zeeman field *h*

To examine the effect of the Zeeman field h, we start from the point $\lambda = f = \mu = 0$. At this point, the Zeeman field leaves the spin sector gapless, and induces a finite spin magnetization. To see this, we write $\phi_s(x) = \tilde{\phi}_s(x) + \frac{\sqrt{2}hK_s}{v_s}x$. Then, in terms of $\tilde{\phi}_s$, the h term in Eq. (6) disappears, and the cosine in the g_s term [Eq. (8)] becomes spatially modulated; the effect of the cosine term is thus suppressed by the Zeeman field. Additionally, there is a constant term in the energy density, $\frac{K_s}{\pi v_s}h^2$. Turning on f and λ, a gapless phase with a finite spin magnetization density appears in a region around the point $f = \lambda = 0$, whose extent depends on h. The critical lines at large λ beyond the points 1 and 2 [thick black lines in Fig. 2(a)] similarly expand into gapless regions upon increasing h. Away from points 1, 2 and the origin $\lambda = f = 0$, the phase diagram with a small nonzero h is similar to that shown in Fig. 2(a). (For brevity, we do not plot the $h \neq 0$ phase diagram here.) In particular, the existence of a MSB phase is stable for sufficiently small h. Similar considerations can be applied for the phase diagram at a nonzero chemical potential, μ.

VI. DISCUSSION

In this work, we described how electron-electron interactions in zigzag carbon nanotubes lead to the formation of correlated insulating phases. The interactions prevent the magnetic field driven gap closing expected based on the single-particle band structure. In particular, over a range of values of spin-orbit coupling and magnetic flux, we predict that the ground state of the carbon nanotube spontaneously breaks the mirror symmetry of the system. Within this MSB phase, adiabatic changes of the flux drive charge and spin currents along the nanotube, providing an observable, distinguishing signature of this phase.

In experiments, the spin-orbit coupling is fixed for a given nanotube. Therefore the applied flux (along with the Zeeman field and chemical potential) is the primary tool for exploring the phase diagram. To assess whether or not the MSB phase can be realized, we must compare the value of the spin-orbit coupling to the critical value λ^* above which the symmetry breaking phase disappears. The value of λ^* is

determined by the competition between the spin-orbit coupling term $\lambda \sin(\sqrt{2}\phi_s)\sin(\sqrt{2}\phi_c)$ in $H_{\lambda,f}$, Eq. (7), and the $g_c \cos(2\sqrt{2}\phi_c)$ term in H_{BS}, Eq. (8). Experimentally, spin-orbit coupling values of up to a few meV have been reported in CNT quantum dots [8,9,18]. In contrast, we estimate the bare value of $\frac{vg_c}{d} = \frac{U_-}{2\pi d} \approx \frac{e^2}{d}$ [see text below Eq. (8)] to be of the order of a few hundred meV. Therefore it is likely that in experiments, $\lambda < \lambda^*$. Notice that the potential U_- depends on subtle many-body effects and is sensitive to details such as the distance to a gate and its screening properties, as well as screening from high-energy modes of the nanotube that are not included in our model. A quantitative numerical estimate for the value of λ^* is therefore out of reach. Nonetheless, given the large separation of characteristic scales between the Coulomb energy and SOC, our prediction of $\lambda < \lambda^*$ is robust and indicates that the MSB phase may be accessible in experiments. However, whether the MSB phase is realized also depends on the strength of the Zeeman term h, which is not independent of the orbital magnetic flux Φ (notice that $h \neq 0$ when $\Phi = \Phi_c$). Therefore, as Φ is swept across Φ_c, the system either enters the MSB phase, or a phase with a nonzero spin magnetization and gapless spin excitations. In either case, the charge gap remains open, in agreement with the experimental observation [21]. In view of future experiments, closing of the spin gap near $\Phi = \Phi_c$ could be detected via the associated enhancement of magnetic field fluctuations.

[1] I. Shapir, A. Hamo, S. Pecker, C. P. Moca, O. Legeza, G. Zarand, and S. Ilani, Science **364**, 870 (2019).

[2] M. Bockrath, D. H. Cobden, J. Lu, A. G. Rinzler, R. E. Smalley, L. Balents, and P. L. McEuen, Nature (London) **397**, 598 (1999).

[3] R. Leturcq, C. Stampfer, K. Inderbitzin, L. Durrer, C. Hierold, E. Mariani, M. G. Schultz, F. von Oppen, and K. Ensslin, Nat. Phys. **5**, 327 (2009).

[4] A. Benyamini, A. Hamo, S. Viola Kusminskiy, F. von Oppen, and S. Ilani, Nat. Phys. **10**, 151 (2014).

[5] H. Suzuura and T. Ando, Phys. Rev. B **65**, 235412 (2002).

[6] E. Mariani and F. von Oppen, Phys. Rev. B **80**, 155411 (2009).

[7] N. M. Gabor, Z. Zhong, K. Bosnick, J. Park, and P. L. McEuen, Science **325**, 1367 (2009).

[8] F. Kuemmeth, S. Ilani, D. C. Ralph, and P. L. McEuen, Nature (London) **452**, 448 (2008).

[9] G. A. Steele, F. Pei, E. A. Laird, J. M. Jol, H. B. Meerwaldt, and L. P. Kouwenhoven, Nat. Commun. **4**, 1573 (2013).

[10] K. Flensberg and C. M. Marcus, Phys. Rev. B **81**, 195418 (2010).

[11] S. Weiss, E. I. Rashba, F. Kuemmeth, H. O. H. Churchill, and K. Flensberg, Phys. Rev. B **82**, 165427 (2010).

[12] E. A. Laird and L. P. Kouwenhovern, Nat. Nanotechnol. **8**, 565 (2013).

[13] D. V. Bulaev, B. Trauzettel, and D. Loss, Phys. Rev. B **77**, 235301 (2008).

[14] K. M. Borysenko, Y. G. Semenov, K. W. Kim, and J. M. Zavada, Phys. Rev. B **77**, 205402 (2008).

[15] H. O. H. Churchill, F. Kuemmeth, J. W. Harlow, A. J. Bestwick, E. I. Rashba, K. Flensberg, C. H. Stwertka, T. Taychatanapat, S. K. Watson, and C. M. Marcus, Phys. Rev. Lett. **102**, 166802 (2009).

[16] M. S. Rudner and E. I. Rashba, Phys. Rev. B **81**, 125426 (2010).

[17] A. Pályi, P. R. Struck, M. Rudner, K. Flensberg, and G. Burkard, Phys. Rev. Lett. **108**, 206811 (2012).

[18] E. A. Laird, F. Kuemmeth, G. A. Steele, K. Grove-Rasmussen, J. Nygård, K. Flensberg, and L. P. Kouwenhoven, Rev. Mod. Phys. **87**, 703 (2015).

[19] C. L. Kane and E. J. Mele, Phys. Rev. Lett. **78**, 1932 (1997).

[20] M. Ouyang, J.-L. Huang, C. L. Cheung, and C. M. Lieber, Science **292**, 702 (2001).

[21] V. V. Deshpande, B. Chandra, R. Caldwell, D. S. Novikov, J. Hone, and M. Bockrath, Science **323**, 106 (2009).

[22] R. Egger and A. O. Gogolin, Phys. Rev. Lett. **79**, 5082 (1997).

[23] L. Balents and M. P. A. Fisher, Phys. Rev. B **55**, R11973 (1997).

[24] Y. A. Krotov, D.-H. Lee, and S. G. Louie, Phys. Rev. Lett. **78**, 4245 (1997).

[25] J. E. Bunder and H.-H. Lin, Phys. Rev. B **78**, 035401 (2008).

[26] M. Rontani, Phys. Rev. B **90**, 195415 (2014).

[27] D. Varsano, S. Sorella, D. Sangalli, M. Barborini, S. Corni, E. Molinari, and M. Rontani, Nat. Commun. **8**, 1461 (2017).

[28] Y. Efroni, S. Ilani, and E. Berg, Phys. Rev. Lett. **119**, 147704 (2017).

[29] W. P. Su, J. R. Schrieffer, and A. J. Heeger, Phys. Rev. Lett. **42**, 1698 (1979).

[30] T. Giamarchi, *Quantum Physics in One Dimension* (Oxford University Press, Oxford, 2003).

[31] C. Kane, L. Balents, and M. P. A. Fisher, Phys. Rev. Lett. **79**, 5086 (1997).

[32] R. D. King-Smith and D. Vanderbilt, Phys. Rev. B **47**, 1651 (1993).

[33] R. Resta, Rev. Mod. Phys. **66**, 899 (1994).

[34] R. Resta, Phys. Rev. Lett. **80**, 1800 (1998).

[35] N. Marzari, A. A. Mostofi, J. R. Yates, I. Souza, and D. Vanderbilt, Rev. Mod. Phys. **84**, 1419 (2012).

[36] J. K. Asboth, L. Oroszlany, and A. Pályi, *A Short Course on Topological Insulators: Band-Structure Topology and Edge States in One and Two Dimensions*, Lecture Notes in Physics Vol. 919 (Springer, Switzerland, 2016).

[37] L. S. Levitov and A. M. Tsvelik, Phys. Rev. Lett. **90**, 016401 (2003).